WINDMI Optimization and Performance Validation

R.S. Weigel, W. Horton
Institute for Fusion Studies, The University of Texas at Austin
Austin, Texas 78712

and I. Doxas
Department of Physics, University of Colorado
Boulder, Colorado 80309–0391 USA

July 13, 2000

Abstract

An optimization study of the prediction performance for the substorm model WINDMI is presented. The model is based on the Earth's magnetospheric dynamics and provides a low order description of the nightside energy loading and unloading that takes place during the substorm process. Previous studies of this model on isolated substorms have indicated that it can be a good predictor of solar wind driven substorm activity as measured by fluctuations in the AL index for selected substorms. Because the model is based on a set of VB_s driven nonlinear ordinary differential equations which can exhibit bifurcation and catastrophe like behavior, an optimization of the model using conventional minimization techniques over a large data set does not work well. For such systems the genetic algorithm method of optimization is more efficient at exploring the parameter space. We present the results of a genetic algorithm optimization of WINDMI using the Blanchard–McPherron and the Bargatze data set and test statistically alternative forms of the model which include the effects of ionospheric conductivity enhancements and region 2 coupling. A key result from the large scale computations used to search for a uniform convergence of the prediction over the 117 substorm database, is the finding that there are three distinct types of VB_s-AL wave forms characterizing the substorms in the Blanchard–McPherron database. Two types are given by the internally triggered WINDMI model and the third type requires an external trigger such as the northward turning of the IMF model of Lyons 1995.

1 Introduction

In view of the success of the low order description of magnetospheric dynamics which uses a truncated description of the energy transfer process during a substorm, it is desirable to have a reliable method for optimizing such models over a large historical data set. Two such models are the Faraday loop model [*Klimas et al.* 1994] and WINDMI [*Horton and Doxas* 1996, 1998]. In contrast to filter based models which are also used to predict substorm activity, these models are more difficult to optimize because they can exhibit properties of self organization and bifurcations. For this reason, optimization of physics based models is more difficult because these models have a high density of local minima in the error landscape and thus require a global search method. For filter based models, including local–linear [*Vassiliadis et al.* 1994] and neural network [*Weigel et al.* 1999] filters, the optimization is more straightforward. In the case of linear and local–linear models a matrix inversion technique exists which provides the desired minimum error [*Box and Jenkins*, 1976]. For neural network models, a standard backpropagation minimization algorithm can be used [*Bishop*, 1995].

In this work we report on the determination of the optimum parameters of the low order physics model WINDMI which describes the relationship between the energy storage and unloading in the magnetosphere during a substorm. The model contains a concise description of the internal trigger mechanism that occurs from the near–Earth neutral line model. The model appears consistent with the dynamics observed in the global MHD simulations. This internally triggered unloading event is what we will refer to as a type I substorms which gives the globally correlated magnetospheric signatures widely recognized to account for many substorm characteristics (*Baker et al.*, 1999). A type I substorm from the database analyzed here is shown in the left panel of Fig. 1. Previous evaluations of this model done in the context of individual substorms showed good performance of the model and qualitative agreement with the Farrugia 30 hr, slowly rotating large IMF magnetic cloud [*Farrugia et al.* 1993] event evaluated by *Horton et al.* [1998] in which the minimization was done by perturbing the base line parameters from their mean values on an individual substorm. The baseline values of the physics parameter vector $\mathbf{P}$ were calculated by *Horton and Doxas* (1996, 1998) using standard magnetospheric physics models.

Perhaps one of the most useful reasons for having a systematic method for minimization is that modifications to the model in terms of effects which were omitted can be evaluated and tested

against a database to determine if they have a statistically significant effect on the performance of the model. In this paper, two modifications to the model are considered and the effect of their inclusion is evaluated. The evaluation consists of posing the question as to how low the error metric measuring the difference between the predicted $\widehat{AL}$ and the measured AL can be driven for the physics parameters within the standard range of acceptable values.

The first modification which we consider is the inclusion of ionospheric conductivity enhancement due to electron precipitation. The ionospheric conductivity enhancement is based on the relation between the precipitating electron energy flux Φ_E and height integrated Hall and Pederson conductivity as given by *Robinson et al.* [1988]. The second modification to the model is the inclusion of an energy coupling to nightside region 2 currents based on the model described by *Siscoe* [1982].

In Section 2 we give the WINDMI model, describe how the parameters are estimated, and list reference values for each of the physics based parameters. In Section 3 we discuss the data sets for which the minimization is performed and consider the limits of predictability and resolution of the time series in terms of the standard measure of the prediction error. After reviewing and evaluating three methods for minimization in Section 4, we describe in Section 5 the results of using a genetic algorithm based minimization method on the reference model. The physics behind the two modifications to the model are then described and their effect on performance is given in the discussion and conclusion in Section 6.

2 Model description

We start with the reference model of WINDMI as developed in *Horton and Doxas* [1996,1998] which conserves charge and energy and describes the causal energy transfer processes in the coupled magnetosphere–ionosphere during substorms. The mathematical expression of the model is given in Eqns. 1 - 6 and an energy flow diagram of the multiple energy pathways is given in *Horton et al.*, [1999]. The model describes six distinct (and comparable) energy components with six pairs of energy transfer terms. The driven–damped nonlinear system of six ordinary differential equations (ODEs) is

$$L\,\frac{dI}{dt} = V_{\rm sw} - V + M\,\frac{dI_1}{dt} \tag{1}$$

$$C\,\frac{dV}{dt} = I - I_1 - \alpha P^{1/2} - \Sigma V \tag{2}$$

$$\frac{3}{2}\,\frac{dP}{dt} = \Sigma\,\frac{V^2}{\Omega} - u_0\,K_{\parallel}^{1/2}\Theta(I - I_c)P - \frac{P}{\tau_E} \tag{3}$$

$$\frac{dK_{\parallel}}{dt} = \alpha P^{1/2} V - \frac{K_{\parallel}}{\tau_{\parallel}} \tag{4}$$

$$L_1\,\frac{dI_1}{dt} = V - V_1 + M\,\frac{dI}{dt} \tag{5}$$

$$C_1\,\frac{dV_1}{dt} = I_1 - \Sigma_I V_1. \tag{6}$$

Equations 1 and 2 describe the evolution of the cross tail potential $V = E_y L_y$ and cross tail current I given the solar–wind driving potential $V_{\rm sw} = \beta v_x B_s L_y$ where the factor β represents the efficiency with which the solar–wind voltage is translated to a cross–tail potential drop. The system of Eqns. 1 - 6 provide a faithful prediction of the standard type I isolated substorm as shown in Horton *et al.* [1999] and earlier works.

A careful case by case examination of the phase of the region 1 current increase with respect to the change in the convection electric field shows that the WINDMI model with an internal trigger (triggered when the cross–tail current reaches a critical level, I_c) cannot produce what we call a type II substorm. An example for the type II substorm is shown in Fig. 2 where we see that there is first a sharp drop in the convection electric field and then an increase in the westward electrojet current. The $I_1 - V$ phase diagrams for the standard internal trigger model always have have the reverse time sequence of the the two signals as forced by the Kirchhoffian structure of the equations. Therefore, we conclude that the type II events must be triggered by an abrupt drop of the convection electric field. This drop of the convection electric field is a straightforward consequence of an abrupt northward turning of the IMF. This is the scenario envisioned by Lyons 1995 and used recently by Blanchard and Lyons 2000 to model a new database. Here, by using the genetic algorithm (GA) minimization technique, we can rule out the possibility that we previously thought might explain these events with large error (ARV) measures as being substorms for which the the minimization was stuck in a local minimum. After making long runs (5–10 hrs. with 100 initial population vectors) with the GA method we are confident that there are a set of events for which an external trigger mechanism is to be inferred from the results of the minimization studies.

The WINDMI model goes beyond the linear circuit based models of the interaction of the

geotail current I loop and nightside region 1 current I_1 loops through the mutual inductance M by including the plasma physics of the internal trigger for unloading pressure through parallel flows on newly opened magnetic field lines. The pressure unloading switch is based on a model of the bifurcation of the magnetic field that occurs when the cross–tail current (or current density $j_y(t) = I(t)/L_x L_z$) reaches a critical level, I_c in Eq. 3. The total plasma current is the sum of the pressure gradient current $I_{ps} \propto P^{1/2}$ and the collisionless viscous stress driven current $I_{vis} \propto \Sigma V$ driven by plasma convection through the off–diagonal momentum stress tensor (*Horton and Doxas*, 1996).

The reference model includes an explicit magnetosphere–ionosphere coupling given by Eqns. 5 and 6. These two equations describe the inductive coupling between the lobe current and field aligned region 1 currents. This is in contrast to simplified models which assume that the magnetic field lines connecting the magnetosphere to the ionosphere are equipotentials so that the magnetospheric and ionospheric electric fields are proportional with the proportionality determined by a mapping factor *Weimer* [1994]. In the context of WINDMI this proportionality holds when both the rate of change of the field aligned current and cross–tail plasma sheet current (I_1 and I, respectively) are small, or more generally, when the condition for the ionospheric current loop with self–inductance L_1 and mutual inductance M is that $|L_1 dI_1/dt - M dI/dt| \ll |V - V_1|$ in Eqn. 5. A plot of V_1 versus V during a substorm cycle shows that $V_1 \simeq V$ except for a few minute periods during the expansion phase where V_1 lags V.

The set of dynamical variables is $\mathbf{x} = (I, V, P, K, I_1, V_1)$, and the 14 parameters, which will be taken as constant in first order approximation, are given by $\mathbf{P} = (L, M, C, \Sigma, \Omega, u_o, I_c, \alpha, \tau_{\|}, \tau_E, L_1, C_1, \Sigma_I, \beta)$. Note that the number of free parameters can be reduced by 3 if the equations are written in dimensionless form [*Smith et al.* 2000]. We choose to work with the full dimensional set of equations to compare with earlier published works and data.

In this work we consider the error minimization of WINDMI with respect to the parameter set $\mathbf{P}$. The values of these parameters are restricted since they are based on estimates of magnetospheric quantities such as effective inductances, capacitances and relaxation time scales. The actual magnitudes may vary in time, since, for example, the lobe cross sectional area changes during the course of a substorm which changes the lobe inductance L. In the reference model, which is intended to be a lowest order approximation, all of the parameters are assumed fixed. In Section 5 we allow the ionospheric conductivity Σ_I to vary using two models which describe its evolution in

terms of the dynamical variables.

A direct physics estimate of the lobe inductance and the plasma sheet capacitance taken from Horton and Doxas [1996] is given as an example. From a magnetic field model such as Tsyganenko 1996 we can calculate the lobe area A and the effective length L_x of the support of the geotail current density $j_y(x)$, then

$$\mathcal{L} = \mu_o A/L_x = 40H \tag{7}$$

for $A = \pi(10R_E)^2$ and $L_x = 60R_E$. Assuming an uncertainty in A and L_x of $\pm 10\%$ each gives a range of the lobe inductance of $\delta\mathcal{L} = \pm 8H$. *Horton et al.* [1998] use Tsyganenko to compute with more precision the electrical parameters as a function of the IMF angle, but the variation is not large. Since the plasma polarization ρ_m/B^2 is strongly peaked on the equatorial plane, the central plasma sheet capacitance C follows from the total $\mathbf{E}\times\mathbf{B}$ flow kinetic energy $K_\perp = \frac{1}{2}\int \rho(x,z)\frac{E_y^2}{B^2}d^3x \equiv \frac{1}{2}CV^2$. The integral is easily evaluated using $B^2 = B_z^2 + B_x'^2 z^2$ which is valid for $|z| < 3R_E$ and gives

$$C = \frac{\pi\rho_m(0)}{B_z B_{xo}}\frac{L_x L_z}{L_y} = 12000F \tag{8}$$

Here $\rho_m(0)$ is the mass density at the equatorial plane. As a result of the dependency of the plasma sheet capacitance on B_z, B_{xo}, and $\rho_m(0)$ which vary greatly during a substorm, we allow for a large range capacitances when optimizing. The fundamental magnetotail cavity period is $T = 2\pi(\mathcal{L}C)^{1/2} \simeq 1$ hr (*Horton et al.* [1998]).

In Table 1 we list estimated values of all magnetospheric parameters in the reference model. These estimates have been derived and calculated previously by *Horton and Doxas* [1996, 1998].

3 Substorm Data Sets

3.1 The Blanchard–McPherron dataset

We use the Blanchard-McPherron data base of 117 isolated substorms which provides 1 min. resolution of both AL and $v_x B_s$. This data set has been studied in the context of a five parameter linear prediction filter model [*Blanchard and McPherron* 1995; *Smith and Horton*, 1998] with a minimum ARV of 0.29 when a set of five optimal parameters is determined for each of the substorm intervals. When the average of each parameter over all the intervals is used the ARV increases to 0.53.

It is important to note that one of the criteria used for classification as an isolated substorm is based on the behavior of the solar wind. In order to be classified as an isolated substorm there

must be a southward turning of the IMF after a quiet period. Then, either the level of the solar wind energy input (which is greatly enhanced during periods of southward IMF) must stay at a low level ($V_{\rm sw} \leq 60$kV), or the IMF must turn northward after the expansion phase. These criteria are required so that there is a clear signature of a substorm recovery phase. If the solar–wind energy input remains high after the expansion phase then the event will be classified as either a magnetic storm, or a case of a complex substorm with intensifications.

3.2 The Bargatze dataset

The 34 data sets studied and compiled by *Bargatze et al.* [1995] from which the interplanetary magnetic field and solar wind velocity were measured by the IMP8 spacecraft were sorted in order of increasing activity levels. Each of the 30 intervals contains multiple substorms at a time resolution of 2.5 minutes. The lowest value of ARV found by *Bargatze et al.* on this data set using a linear prediction filter was 0.55. *Weigel et al.* [1999] used a neural network based filter on this data set in which the input was given by 15 minute delayed values of AL and VB_s to obtain an ARV of 0.20 using a gated network. Note that this value of ARV is not directly comparable to that obtained from the linear filter by *Bargatze et al.* or the WINDMI model since the neural network uses the past values of AL as an input whereas the linear filter and WINDMI use only the solar–wind voltage VB_s. The filter inputs for the neural net were the 15 min time delayed values of AL as well as 15 min delayed values of VB_s while the *Bargatze et al.* linear filters use only the VB_s signal as the input. Therefore, any filter which uses measured historical values of AL will have improved performance due to the autocorrelation between the signal and its time delayed value.

The major difference between the *Blanchard and McPherron* (dataset 1) dataset and the one provided by *Bargatze et al.* (dataset 2) is in how the events were put together. Dataset 1 contains one substorm per interval. Dataset 2 typically has many substorm events per interval and within each interval the events must have near equal AL index magnitudes. The effect of having multiple substorms per interval will become apparent when the optimization is done. Since we will determine an ideal set of parameters for each interval, we expect that the longer intervals, having multiple events will have an error that is higher.

4 Optimization methods

There are many ways to approach a given minimization problem and the method used is highly dependent on the problem. The most common minimization methods are least squares minimization or gradient descent methods which are most often used for minimizing linear and neural network type filters. Here we are attempting to optimize the parameters of a nonlinear set of differential equations which have a wide variety of possible dynamics including limit cycles, chaotic attractors and fixed points. In addition, the system is forced by the solar–wind which has a stochastic component, thus increasing the complexity of the possible output dynamics. Since this type of minimization which involves optimizing the parameters of a nonlinear set of differential equations is not a standard problem we describe several possible approaches and their advantages and disadvantages before presenting the results.

4.1 Grid and Random Search Optimization

The grid search procedure is implemented by splitting the parameter ranges shown in Table 2 into three values given by the min, max and mean(min,max). These parameter ranges are determined by estimates of the maximum and minimum possible values based on physics estimates of the relevant variables. Given each of parameters has three values to be tested, and that there are 14 parameters, we test all $3^{14} \simeq 4.8 \cdot 10^6$ combinations by parallelizing the error calculation code which integrates the 6 ODE system and then calculates the ARV between the predicted $\widehat{AL}$ output and the actual AL output. This is realized by creating a list of the all the possible parameter vectors and splitting this large set into $N_{\text{processors}}$ pieces. Run in this way, the number of computations is scaled to $3^{14}/N_{\text{processors}}$. Using the Cray T3E with $N_{\text{processors}} = 80$ processing elements, this computation required approximately 24 hrs per substorm interval.

The random search method we split each parameter range into three pieces, but the three values in the range are chosen at random. The parallelized calculation procedure is the same as that for the grid search method.

We found that the random search method produced nearly the same optimized parameter set as the faster but more sophisticated genetic algorithm method discussed below in Sect. 4.3.

4.2 Gradient Descent Optimization

The elementary gradient descent algorithm uses the following rule for updating the elements of a parameter (or weight) vector, w_i to minimize an error function, $\mathcal{E}$.

$$w_i^{\tau+1} = w_i^{\tau} - \frac{\partial \mathcal{E}}{\partial w_i} \tag{9}$$

For the minimization of WINDMI the w_i's are the set of 14 physics parameters given in Table 2. The error function is taken to be the average relative variance (ARV) between the measured signal, AL_i and the predicted signal $\widehat{AL_i}$ defined by

$$ARV = \frac{\frac{1}{N}\sum_{i=1}^{N}(AL_i - \widehat{AL_i})^2}{\sigma_{AL}^2} \tag{10}$$

which is interpreted as the fraction of the variance of the time series which is not predicted. This is related to the often used "prediction efficiency" (PE) by $ARV = 1 - PE$. Another often used performance statistic used in time series prediction studies is the correlation coefficient, ρ. If the measured AL and the predicted $\widehat{AL}$ have the same variance and mean, and the errors $e_i = AL_i - \widehat{AL_i}$ are uncorrelated with AL, then $ARV = 1 - \rho^2$. Since this is usually satisfied, the correlation coefficient does not give additional information about the prediction performance and is therefore not reported.

There are several modifications which can be made to speed the convergence of the basic gradient descent method, for example, by adding acceleration or inertial terms or using a conjugate gradient method. The choice method used is dependent on the type of problem being considered. The methods based on gradient descent minimization are appropriate for error landscapes which have only one global minimum. If only few local minimum exist, then the algorithm can be restarted several times with different initial conditions. Since the error landscape has many local minimum, this method becomes inefficient and a global method such as a genetic algorithm, which allows for movement out of local minima, is needed.

4.3 Genetic Algorithm Optimization

Because of the time required for a random grid search is prohibitive since it scales with N_p^N where N is the number of grid points per parameter, and N_p is the number of parameters, and the

gradient descent type algorithms have difficulty when encountering local minima, we turn to a more sophisticated optimization method which will combine the advantages of both methods.

We find the genetic algorithm (GA) minimization method to be a more efficient method for our problem since it allows both searching an error function in which has many local minimum and which has a parameter set which has components which are are not completely independent. The essential features for implementing the algorithm are now outlined.

The problem is to minimize the error function ARV=ARV($\mathbf{P}$) where the parameter vector $\mathbf{P}$ has elements which are the fourteen physics parameters of WINDMI:

$$\mathbf{P} = (P^1, P^2, ..., P^{14}) \tag{11}$$

$$= (\mathcal{L}, \Sigma, C, ..., \Sigma_I) \tag{12}$$

which are bounded by maximum and minimum estimates defined in Table 2

$$\mathbf{P}_{\max} = (\mathcal{L}_{\max}, ..., \Sigma_{I_{\max}}) \tag{13}$$

$$\mathbf{P}_{\min} = (\mathcal{L}_{\min}, ..., \Sigma_{I_{\min}}) \tag{14}$$

(a) Create $2N_{\rm pop}$ "population" vectors $\mathbf{P}_j$ whose elements are random samples in the range $P^i_{\min} \leq P^i \leq P^i_{\max}$

$$\mathbf{P}_1 = (\mathcal{L}^1, ..., \Sigma^1_I) \tag{15}$$

$$\vdots \tag{16}$$

$$\mathbf{P}_{2N_{\rm pop}} = (\mathcal{L}^{2N_{\rm pop}}, ..., \Sigma_I^{2N_{\rm pop}}) \tag{17}$$

(b) Calculate the error measure ARV($\mathbf{P}_j$) ($j = 1 \ldots 2N_{\rm pop}$) and keep only half of the vectors ($N_{\rm pop}$) corresponding to the lowest error.

(c) Mate these two population and create a new generation of $\mathbf{P}_j$ by

- Randomly choosing $N_{\rm pop}/2$ mating pairs which will give $N_{\rm pop}$ offspring.
- Randomly choosing a split point $\mathcal{S}$ of parameter vector. ($1 \leq \mathcal{S} \leq 13$) as diagrammed in Fig. 3.

(d) Introduce mutation (which pushes solution out of local minimum) by choosing N_m vectors from $N_{\rm pop}$ and replacing the value of a parameter with a random value in its range.

(e) Repeat (c)–(d) until a stopping criterion is satisfied, for example

$$\overline{ARV}|^{\rm top5} \quad \text{at generation k} \tag{18}$$

$$\approx \overline{ARV}|^{\rm top5} \quad \text{at generation k+1} \tag{19}$$

The stopping criterion is usually found in 4 to 5 generations. In all of the results which follow, we use the genetic algorithm minimization method to determine the optimal parameters. We find that the genetic algorithm minimization method is the most reliable and efficient for minimizing WINDMI, and for this reason all results reported were generated using this scheme.

5 Optimization Results

In this section we show the performance of the reference WINDMI model on several intervals of the Bargatze and Blanchard–McPherron substorm database. First we note that certain substorm intervals have a very low error. For example, consider the following result of minimization on the Blanchard–McPherron interval as shown in Figure 4.

An observation which is made from considering the intervals with the lowest error is that the intervals which are most easily predicted tend to have the classic substorm AL structure with respect to the southward turning of the IMF. An example of the models performance on a classic substorm is shown in Figure 4 (left panel, unoptimized) and Figure 4 (right panel, optimized) above.

Using the maximum and minimum physical parameter values shown in Table 2 we minimize over each of the 117 substorms in the Blanchard and McPherron database and over each of the 34 intervals of the Bargatze database. The ARV distribution for the Blanchard and McPherron databases is shown in Figs. 5. The mean over the Blanchard and McPherron database is 0.93 while the mean over the Bargatze database is 0.97. We see that there are many intervals that are well predicted by the WINDMI model with an internal trigger (86 events with $ARV < 1.0$). Apparently there are two other groups for which the model does poorly: Group 1 with 24 events with $1.0 \leq ARV \leq 2.0$ and 7 intervals in Group 2 with $ARV > 2.0$.

For approximately a year the WINDMI validation problem was that the minimization procedure was not able to find the correct parameter values. After a thorough search using the genetic algorithm method it was determined through a careful case by case examination of the phase of the region 1 current increase with respect to the convection electric field that the WINDMI model with its internal trigger cannot reproduce the type II substorms shown in Fig. 2 where we see that there is first a sharp decrease in the convection electric field and then an increase in the westward electrojet current as measured by the AL index. The I_1–V phase diagrams have the reverse time ordering for an internally triggered event. Therefore, we conclude that these type II events are triggered by an abrupt drop of the convection electric field. This scenario then conforms to the northward turning substorm trigger scenario of *Lyons* [1995].

In Figure 6 the distribution of parameter values is shown for $(\mathcal{L}, M, C, \Sigma)$. Ideally there would be a sharply peaked distribution for each histogram centered around a mean value which is near the reference physics value for each constant. The mean value of each parameter obtained from the minimization over the Blanchard and McPherron database is listed in Table 3.

For prediction purposes it would be valuable to have only one set of parameters which is used for all substorms, unless there exists a method for determining a slowly varying parameter vector $\mathbf{P}$ based on the state space vector $\mathbf{x}(\mathbf{t})$ which varies reflecting different states of the magnetosphere. This has not yet proven possible although more extensive use of other magnetospheric parameters (K_p, IMF, PC, AU) has not been well explored. Instead it seems that a local parameter look–up procedure must be used to obtain satisfactory results. Nonlinear filter based models can easily incorporate a changing parameter set as a function of the input variables. This is the what is done for a local linear network in which the expansion coefficients are dependent on the input variables [*Vassiliadis et al.*, 1994]. It is possible that a network could be used to choose the physics model parameter $\mathbf{P}$ vector given the solar–wind (and recent past values of $\mathbf{P}$) input variables. Here we are interested in the limits of a pure physics model in which the parameter changes are due to physical effects only. Using these mean values from the histograms of the parameters, we find the ARV to for the Blanchard and McPherron dataset to be 1.19 and the ARV of the Bargatze dataset to be 1.53. These are unacceptably large error values.

The wide distributions of the parameter histograms and increase in ARV when using the mean parameter set, $\overline{\mathbf{P}}$ is similar to that encountered when fitting the parameters for linear filter models of substorms. In the linear filter case, the ARV increased from 0.29 to 0.53 when the mean value of

the parameters was used [*Blanchard and McPherron*, 1993]. This is a manifestation of either the intrinsic unpredictability of the M–I system, noise, or effects not included in the modeling. Now we ask if upgrades of the WINDMI98 model with physics which is not included in the reference model to determine if the prediction can improve the performace significantly. In a follow up work we develop a major revision to the WINDMI model with an external trigger. In this work we continue to use the standard internal trigger of WINDMI98.

5.1 Ionospheric conductivity enhancement from Electron Precipitation

The first change to the reference model is to add a nonlinear ionospheric conductivity model. The reference model assumes a constant height integrated ionospheric conductivity, Σ_1, which is independent of electron precipitation energy. Thus, the reference model assumes

$$\Sigma_I = \Sigma_{Io} = \text{constant} \qquad \text{Model A} \tag{20}$$

As is clear from various models of ionospheric conductivity during active times [*Vickrey et al.*, 1981; *Spiro et al.*, 1988; *Gjerloev et al.*, 2000], the Pederson conductivity is a strong function of the electron precipitation energy on the ionosphere. There is also a spatial dependence which we do not attempt to include at this point.

For the present upgrade, we consider a model which incorporates the *Robinson et al.* [1988] relation between the dissipative Pederson conductivity, Σ_1 and the precipitating electron energy flux Φ_E which is $\Sigma_I \propto \Phi_E^{1/2}$.

The electron precipitation power flux $\Phi_E = j_\parallel \Delta V_\parallel$ is expressed in terms of the dynamic variables of WINDMI by assuming an effective cross–sectional precipitation area A_{eff} so that $j_\parallel = I_1/A_{\text{eff}}$. The parallel potential drop $\phi_\parallel$ is determined by using the *Knight* [1973] and *Lemaire and Scherer* [1983] current–voltage relationship for the potential which develops due to a field aligned current

$$\phi_\parallel = \frac{ne^2}{\sqrt{2\pi m_e T_e}} \frac{I_1}{A_{\text{eff}}} + T_e/e \tag{21}$$

valid when $1\text{kV} < \phi_\parallel < 20\text{kV}$. To this we add the inductive emf $V - V_1$ which occurs as transients along the substorm current loop so that using $\Sigma_I \propto \Phi_E^{1/2} = (\frac{\Delta V_\parallel I_1}{A_{\text{eff}}})^{1/2}$ we have the upgraded model B:

$$\Sigma_I = \Sigma_{Io} + \sqrt{|\gamma_1 I_1^2 + \gamma_2 I_1 (V - V_1)|} \qquad \text{Model B.} \tag{22}$$

This form of ionospheric coupling is a simplified form of that used in global MHD simulations *Janhunen et al.* [1998] and models of high–latitude convection patterns *Blomberg et al.* [1988].

All of the constant terms have been absorbed into Σ_{Io} and instead of using estimates of the constants in Eqn. 21 we determine γ_1 and γ_2 more directly by using experimental values which are observed during substorms. We use the estimates of $\gamma_1 = 2 \cdot 10^{-10}$ and $\gamma_2 = 4 \cdot 10^{-8}$ which give a conductivity enhancement of 30 mho when the field aligned current I_1 is 1MA and $V - V_1 = 5$kV which are representative outputs of the model during substorm times.

The net effect of allowing a conductivity enhancement will be to allow for a changing decay time in the I_1 current. This can be seen considering the response of Eqns. 5 and 6 to a impulse input in the cross–tail potential V it can be shown that I_1 will have a characteristic decay time of Σ_1/C_1.

A summary of change in prediction performance over the complete datasets are shown in Table. 4. We find a statistically significant improvement when the nonlinear conductivity model (Model B) is used. Using the reference model with $\Sigma_{Io} = 9.0$ (Model A) the error metric ARV is 0.93. Using Model B, which uses an empirical relationship to determine the increase in ionospheric conductivity when the region 1 current increased, the ARV is reduced to 0.71. The error measure of ± 0.4 is the standard deviation of this mean ARV.

5.2 Region 2 coupling enhancements

The standard model of the M–I coupling in WINDMI does not include the dissipation and magnetic energy storage due to coupling between the substorm currents and region 2 currents which close in the ring current. Here we follow the argument of *Siscoe* [1982] to derive a coupling between the I_1 and I_2 current loops and note how this coupling effects the overall dynamics. Siscoe considers the energy coupling from the R1 to the R2 current loops due to a cross polar cap potential which drives the R1 currents. When the magnetospheric generator voltage $V(t)$ increases, the boundary diameter of the auroral arc tends to shift equatorward. This shift results in a compression of the ring current particles which Siscoe shows to have a shielding time scale of approximately 1 hour. The net effect is that the ring current coupling acts as an additional current loop with an effective inductance L_{RC} and subauroral resistance R_S, auroral resistance R_A, and charge exchange resistance R_{cx} as defined in Fig. 1 of *Siscoe* [1982].

Here we couple this model to WINDMI by identifying the generating voltage as the magnetospheric potential V. Without region 2 coupling currents the filter which relates the cross–tail potential V and current I to the ionosphere is given by

$$L_1 \frac{dI_1}{dt} = V - V_1 + M \frac{dI}{dt} \tag{23}$$

$$C_1 \frac{dV_1}{dt} = I_1 - \Sigma_1 V_1 \tag{24}$$

which is diagrammed in the top half Fig. 7. Note that for clarity, the mutual inductances between the geotail current and the region 1 and region 2 currents have been omitted. To include the effect of ring current energization due to changes in the ionospheric potential as determined by WINDMI, we add the additional loop as shown in the lower half of Fig. 7.

The new system of equations which supplement Eqns. (1–4) reads

$$L_1 \frac{dI_1}{dt} = V - V_1 + M \frac{dI}{dt} \tag{25}$$

$$C_1 \frac{dV_1}{dt} = I_1 - \Sigma_1 V_1 \left(1 + \frac{\frac{1}{R_S \Sigma_1}}{1 + \frac{2R_A}{R_S}} \right) - I_2 \left(\frac{1}{1 + \frac{2R_A}{R_S}} \right) \tag{26}$$

$$L_{RC} \frac{dI_2}{dt} = V_1 \left(\frac{1}{1 + \frac{2R_A}{R_S}} \right) - 2I_2 \left(R_{cx} + \frac{R_A}{1 + \frac{2R_A}{R_S}} \right) \tag{27}$$

We see the first equation is unchanged where $V(t)$ acts as the voltage source. In a steady state the magnetospheric voltage $V(t)$ maps directly to the ionospheric potential V_1. If the voltage source is a step function, then effect of the R2 current will be to increase the rise time and decrease the steady state amplitude of the R1 current.

The following estimates of the four new parameters R_A, R_S, R_{cx}, and L_{RC} are based on the discussion in *Siscoe* [1982]. An estimate of the ring current resistance due to charge exchange with neutrals given by *Lee et al.* [1982] is $R_{cx} \simeq 0.02\Omega$. Since the sub–auroral ionospheric resistance R_S is much larger than the auroral ionospheric resistance $R_A \simeq 0.1\Omega$, the effective inductance of the ring current can be estimated as $L_{RC} \simeq R_A \tau_s$ where $\tau_s \simeq 1$ hr is the shielding time determined by a detailed analysis of the physics [*Southwood*, 1977]. We recognize that this simplified description of region 2 leaves out the change of the coupling efficiency with the polar cap potential given in *Lu and Siscoe* [199X].

With the region 2 coupling there is a new magnetic energy reservoir. The total system energy is given by the sum of the contributions due to

Plasma Sheet bulk flow:

$$\int_{PS} d^3x \frac{1}{2}\rho_m(v_\perp^2 + v_\parallel^2) = \frac{1}{2}CV^2 + K_\parallel \tag{28}$$

Plasma Sheet thermal energy:

$$\int_{PS} d^3x \frac{3}{2}P = \frac{3}{2}\Omega P \tag{29}$$

Ionospheric bulk flow:

$$\int_{I} d^3x \frac{1}{2}\rho_m v_\perp^2 = \frac{1}{2}C_1V_1^2 \tag{30}$$

region-1, region-2 and Lobe Field:

$$\int_{L+R1+R2} d^3x \frac{B^2}{2\mu_0} = \frac{1}{2}LI^2 + \frac{1}{2}L_1I_1^2 + \frac{1}{2}L_{RC}I_2^2 - MII_1 \tag{31}$$

where we have assumed the energy associated with inductive coupling between the R2-loop and R1-R2 is negligible. The total system energy is thus

$$W = \frac{1}{2}CV^2 + \frac{1}{2}C_1V_1^2 + \frac{1}{2}LI^2 + \frac{1}{2}L_1I_1^2 + \frac{1}{2}L_{RC}I_2^2 - MII_1 + K_\parallel + \frac{3}{2}\Omega P. \tag{32}$$

The sole input of energy is due to the solar–wind power input $IV_{\rm sw}$. The dissipation terms are found by computing dW/dt which reads

$$\frac{dW}{dt} = IV_{\rm sw} - \frac{K_\parallel}{\tau_\parallel} - \Omega u_o K_\parallel^{1/2}\Theta(I - I_c) - \Sigma_1 V_1^2\left(1 + \frac{\frac{1}{R_S\Sigma_1}}{1 + \frac{2R_A}{R_S}}\right) - 2I_2^2\left(R_{cx} + \frac{R_A}{1 + \frac{2R_A}{R_S}}\right) \tag{33}$$

The effect of adding a region 2 current loop to the model can be understood by considering the circuit shown in Fig. 7. The I_1 current has an additional path to follow southward through the ionosphere and to the partial ring current. If I_1 suddenly increases, current will only flow through R_S and no current will flow through L_{RC} initially. Thus, initially there is a decrease of the westward flowing current through Σ_1. In addition, the increased current will store magnetic energy while energy which is being dissipated through via westward current which in the model flows though Σ_1. The inclusion of the magnetic energy storage ($\frac{1}{2}L_{RC}I_2^2$) has the effect of shifting the time phase between I_1 and V_1. The strength of adding the *Siscoe* coupling model is that is

provides the transport of magnetotail energy to the ring current. While the *Siscoe* [1982] model oversimplifies the standard $AIME$ model of M–I coupling (*Lu and Siscoe*, [199X]), it still provieds the key physics of the transport of energy to the ring current.

Table 5 lists the results for the minimization done on the dataset. We see that the addition of a region 2 coupling does not have a significant effect on the performance of the WINDMI98 model. In contrast to the addition of a nonlinear ionospheric conductivity, the region 2 coupling modification to the model were all linear. There is a slight decrease in ARV from 0.93 in the reference model to 0.91 when the ring current coupling model is added. This decrease is not statistically significant since the error bars of these values over lap. The error estimate is determined by the standard deviation of the mean.

6 Discussion and Conclusions

This work describes the effort to obtain optimal parameters for the WINDMI physics model with an internal plasma loading–unloading switch based on the near–Earth neutral line model. After extensive minimization studies we still find that there is a significant set ($< 30\%$) of substorm events for which convergence of the model and the data are not achieved. In view of this negative result, we explore two possibilities: (1) further upgrades to the physics of the existing model we shall call WINDMI98 can eliminate the discrepancy (2) that a new external trigger mechanism, such as the abrupt northward turning of the IMF is required. Conclusion (2) is what we believe we have established in a quantitative sense. This conclusion requires the construction of a new WINDMI2000 model which includes an external trigger.

The key point here is that by having a physics modeling, in contrast to a neural network, there are certain causal time ordered sequence of events for the internally triggered unloading events. From the Fig. 7 we see that that approximately 50% of the events are of this type. Another set, type III, which we find to be typically noisy, weak substorms accounts for the contribution 30% with ARV between 1 and 2 and finally the type II events where the phase relations reversed from that of the internal trigger. These type II events can be explained by imposing the external trigger rules. In a separate follow–up study we introduce the WINDMI 2000 model with the two trigger mechanisms triggers, internal and external. We expect to show that now a uniform convergence can be achieved over the database.

Since its introduction, the possibility that several key factors are left out of the WINDMI

model has been noted. This provides the possibility of hypothesis (1) that further upgrades of the internally triggered WINDMI98 could be made to converge over the entire substorm database. We show with two examples that the upgrade does not solve the problem of the type II events.

The two factors we have identified as serious exclusions are the ionospheric conductivity enhancement during active times and the region 2 coupling. We find that allowing the ionospheric conductivity to increase with the energy dissipated in the ionosphere does yield a significant improvement of substorm prediction. Introducing the coupling of the region 1 current to the region 2 current loop with the Siscoe model does not have a significant effect on predictions, however. This result is not surprising because the modifications included the addition of two additional linear equations to the magnetosphere–ionosphere part of the reference model. If the system of equations was linear, then adding additional equations results in increasing the number of degrees of freedom. The inability of the expanded model to improve predictions supports the hypothesis that the substorm process, as described by the $VB_s - AL$ time series has an effective dimension less than 6. Nonetheless, the addition of the Siscoe model allows the WIMDMI model to extend its predictions to the energy deposited into the inner magnetosphere that originates in the solar wind–magnetosphere dynamo.

We have shown that WINDMI can reproduce the $AL-VB_s$ response of substorms with standard growth–expansion phase signatures by optimizing this model on two classic datasets. This result provides a computer algorithm for defining a classic type I substorm. The results presented show that there are type II events with a rapid increase in I_1 after a rapid drop in the driving voltage which are not represented well for any set of parameters. The prediction performance is not at the same level of either linear or nonlinear filter based methods. This can be attributed to the fact that we have constrained the parameter space based on the physics behind the model. The filter based models which we compare with were derived with no restrictions on the range of the weights.

Although the WINDMI performs remarkably well on some substorm intervals, on others the internal trigger will not converge to a low error measure for any set of physical parameters. This shows that there is a second type of substorm event for which an altogether different current–voltage wave form is required. This work clearly suggests there are cases where a switch triggered by a new northward turning external trigger model is needed in the model.

We have evaluated the prediction results of including two additional physical effects and find that on some substorms the improvement is substantial. However, there is still a clear separation

in the data set in terms of intervals for which the model predicts qualitatively the AL behavior and others for which it does not. Inspection of these intervals clearly points to the need for an external trigger mechanism. The reference WINDMI98 model includes a trigger which is turned on when the lobe current reaches a critical level; this is in agreement with the loading–unloading physics of substorms and global simulations. We believe a critical factor which will improve performance is the inclusion of the physics of a substorm being triggered by an abrupt reduction of the solar wind dynamo drive or northward turning of the IMF. In the future this method will be used to optimize the model.

By use of large scale computations with several optimization methods, we have eliminated the possibility that the disagreement in the type II events arise from the use of unsuitable parameters. Instead, the remaining disagreement arises from the fundamental differences in the wave forms. This quantitative demonstration of the convergence for certain events and the lack of convergence for others is strong, objective evidence for the existence of intrinsically different types of substorm triggering events.

Acknowledgments

The work was supported by the NSF Grant No. ATM-9907637, and NASA Grant NAG5-6198. Computing resources were provided by the Texas Advanced Computing Center (TACC).

References

[1] Bargatze, L.F., D.N. Baker, R.L., McPherron and E.W. Hones, Magnetospheric response to the IMF: substorms, *J. Geophys. Res.*, **90**, 6387, 1985.

[2] Bishop, C.M., *Neural networks for pattern recognition*, Oxford University Press, 1995.

[3] Blanchard, G.T. and R.L. McPherron, A bimodal representation of the response function relating the solar wind electric field to the AL index, *Adv. Space Res., 13*, 71, 1993.

[4] Blomberg, L.G., and G.T. Marklund, The influence of conductivities consistent with field–aligned currents on high–latitude convection patterns, *J. Geophys. Res.*, **93**, 14493, 1988.

[5] Box, G.E.P. and G.M Jenkins, Time series analysis: forecasting and control, San Francisco, Holden-Day, 1976.

[6] Doxas, I. and W. Horton, Magnetospheric dynamics from a low–dimensional nonlinear dynamics model,*Physics of Plasmas*, **6**, 3, 1-7, 1999.

[7] Farrugia, C.J., M.P. Freeman, L.F. Burlaga, R.P. Lepping, and K. Takahashi, The earth's magnetosphere under continued forcing: Substorm activity during the passage of an interplanetary magnetic cloud, J. Geophys. Res. **98**, 7657 (1993).

[8] Kamide, Y. and W. Baumjohann, Magnetosphere–Ionosphere Coupling, Physics and Chemistry in Space, **23**, Springer–Verlag, 1993.

[9] Knight, S., Parallel electric fields, *Planet. Space Sci.*, **21**, 741, 1973.

[10] W. Horton, M. Pekker, and I. Doxas, Magnetic energy storage and the nightside magnetosphere–ionosphere coupling, *Geophys. Res. Lett.*, **25**, 4083 (1998).

[11] Horton, W., I. Doxas, A low-dimensional dynamical model for the solar wind driven geotail-ionosphere system, *J. Geophys. Res.*, 103, A3, 4561, 1998.

[12] Horton, W., J.P. Smith, R. Weigel, C. Crabtree, I. Doxas, B. Goode,and J. Cary, The solar–wind driven magnetosphere–ionosphere as a complex dynamical system, *Physics of Plasmas*, **6**, 11, 1-7, 1999.

[13] Horton, W., M. Pekker, and I. Doxas, "Magnetic energy storage and the nightside magnetosphere-ionosphere coupling," Geophys. Res. Lett. **25**, 21, 4083–4086 (1998).

[14] Janhunen, P., Amm, O. and Greenwald, R.A., Adaptive mesh in global magnetosphere simulation: Comparisons with global convection, *Physics of Space Plasmas*, **15**, 1998.

[15] Klimas, A.J., D.N. Baker, D. Vassiliadis, and D.A. Roberts, Substorm recurrence during steady and variable solar wind driving: Evidence for a normal mode in the unloading dynamics of the magnetosphere, *J. Geophys. Res.*,**99**A8, 14855, 1994.

[16] Lemaire, J., and M. Scherer, Field–aligned current density versus electric potential characteristics for magnetospheric flux tubes, *Annales Geophysicae*, **1**, 91, 1983.

[17] Lyons, L.R., A new theory for magnetospheric substorms, *J. Geophys. Res.*, **100**, 19,069, 1995.

[18] Press, W.H., S.A. Teukolsky, B.P. Flannery, Numerical Recipes in C, Cambridge University Press, 1992.

[19] Robinson, R.M., R.R. Vondrak, K. Miller, T. Dabbs, and D. Hardy, On calculating ionospheric conductances from the flux and energy of precipitating electrons, J. Geophys. Res. **92**, 2265–2569 (1988).

[20] Smith, J.P. and W. Horton, Analysis of the bimodal nature of solar wind–magnetosphere coupling, *J. Geophys. Res., 103A7*, 14917, 1998.

[21] Smith, J. P., J.-L. Thiffeault, and W. Horton, Dynamical range of the WINDMI model: An exploration of possible magnetospheric plasma states, *J. Geophys. Res.*, **105**A6, 12,983, 2000.

[22] Siscoe, G.L., Energy coupling between regions 1 and 2 Birkeland current systems, *J. Geophys. Res.*, **87 A7**, 5124, 1982.

[23] G.L. Siscoe and Lu, G., Energy transfer via region 2 currents: A test of the standard magnetosphere-ionosphere coupling theory, **103A3**, *J. Geophys. Res.*, 1998.

[24] Vassiliadis, D. A., A. J. Klimas, D. N. Baker, and D. A. Roberts, A description of solar wind-magnetosphere coupling based on nonlinear filters, *J. Geophys. Res.*, 99, 3495, 1994.

[25] Weigel R.S., W. Horton, T. Tajima, and T. Detman, Forecasting auroral electrojet activity from solar wind input with neural networks Geophys. Res. Lett. **26**, 1353 (1999).

[26] Southwood, D.J., The role of hot plasma in magnetospheric convection, *J. Geophys. Res.*, **82**, 5512, 1977.

[27] Spiro, R.W., P.H. Reiff, and L.J. Maher, Jr., Precipitating electron flux and auroral zone conductances – an empirical model, *J. Geophys. Res.*, **87 A10**, 8215, 1982.

[28] Vose, M.D., The simple genetic algorithm : foundations and theory, Cambridge, MA, 1999.

[29] Weimer, D.R., Substorm time constants, *J. Geophys. Res., 99A6*, 11005, 1994.

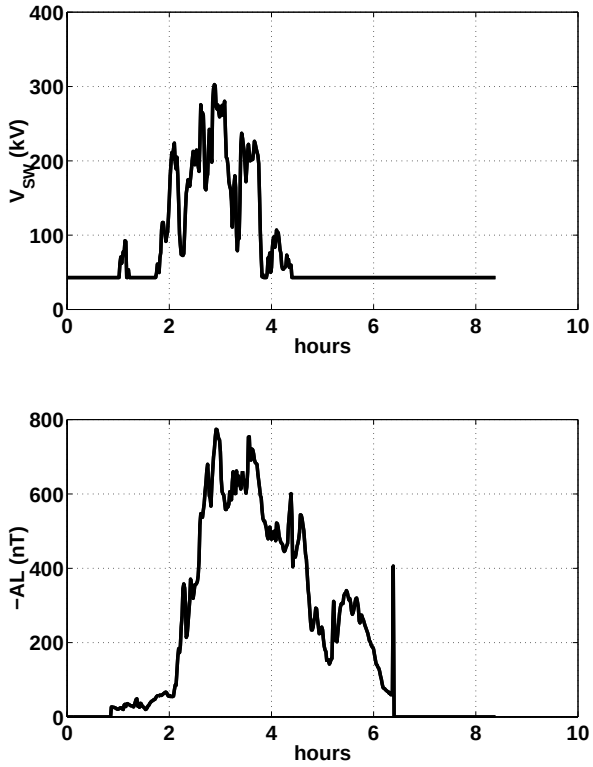

Figure 1: Type 1 substorm example (Blanchard–McPherron dataset A280079

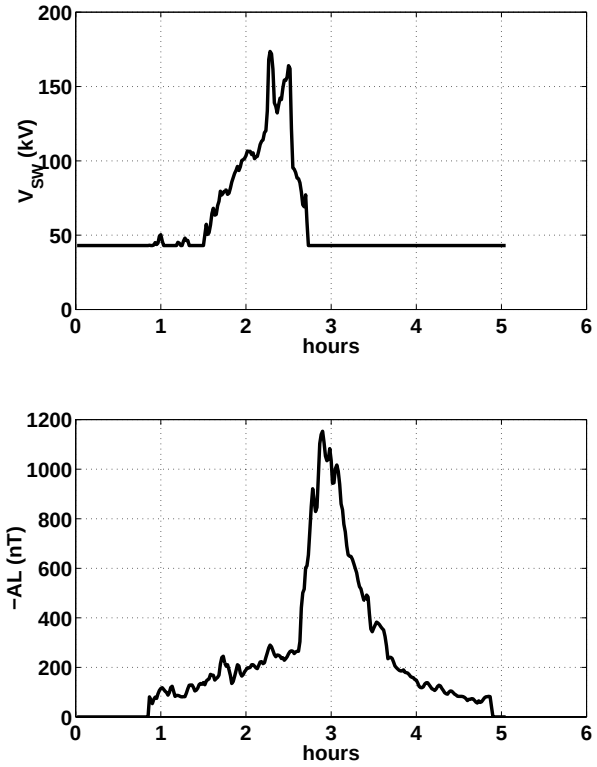

Figure 2: Type 2 substorm example showing first a sharp drop in $V_{\rm sw}$ and then an increase in the westward electrojet current (Blanchard–McPherron dataset A150878

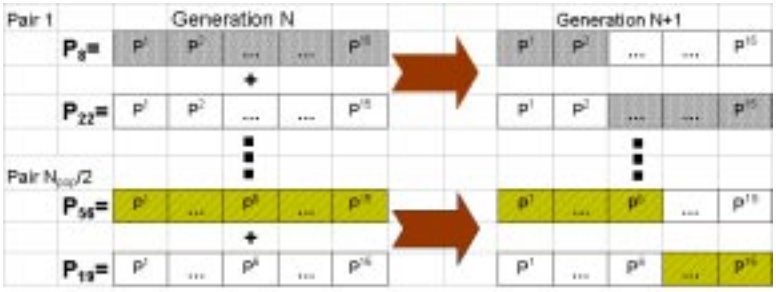

Figure 3: Diagram of genetic algorithm mating procedure. Randomly chosen parameter vectors from an initial generation are combined to form a new generation of parameter vectors. The choice of split position $\mathcal{S}$ is denoted by a color break is chosen at random for each mating pair.

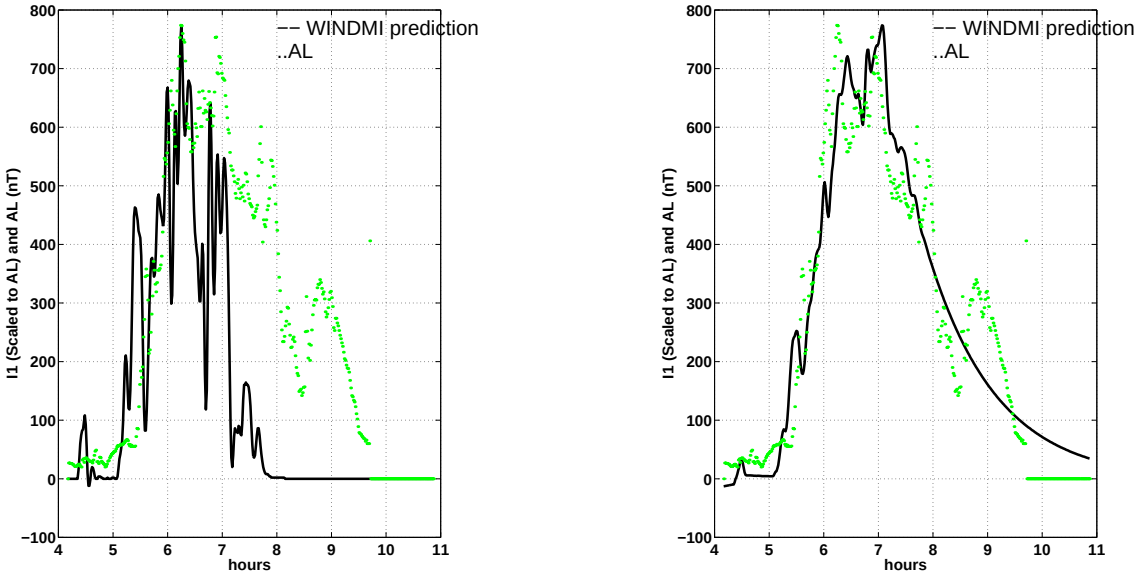

Figure 4: Left Panel: WINDMI prediction of Blanchard–McPherron substorm 04280079 before minimization by genetic algorithm using a randomly chosen parameter set. The ARV over the interval is 0.87 Right Panel: WINDMI prediction of substorm after determining the optimal parameter set using the genetic algorithm for minimization. The ARV over the interval is 0.11.

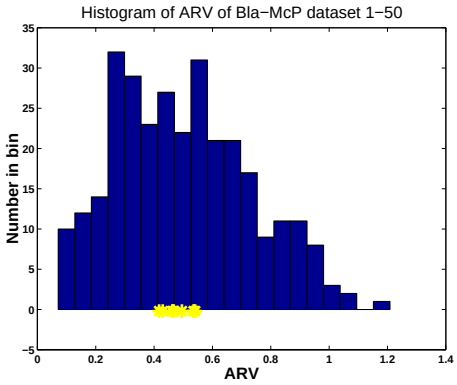

Figure 5: ARV distribution over 117 substorm intervals in the Blanchard and McPherron database. The mean ARV is 0.93.

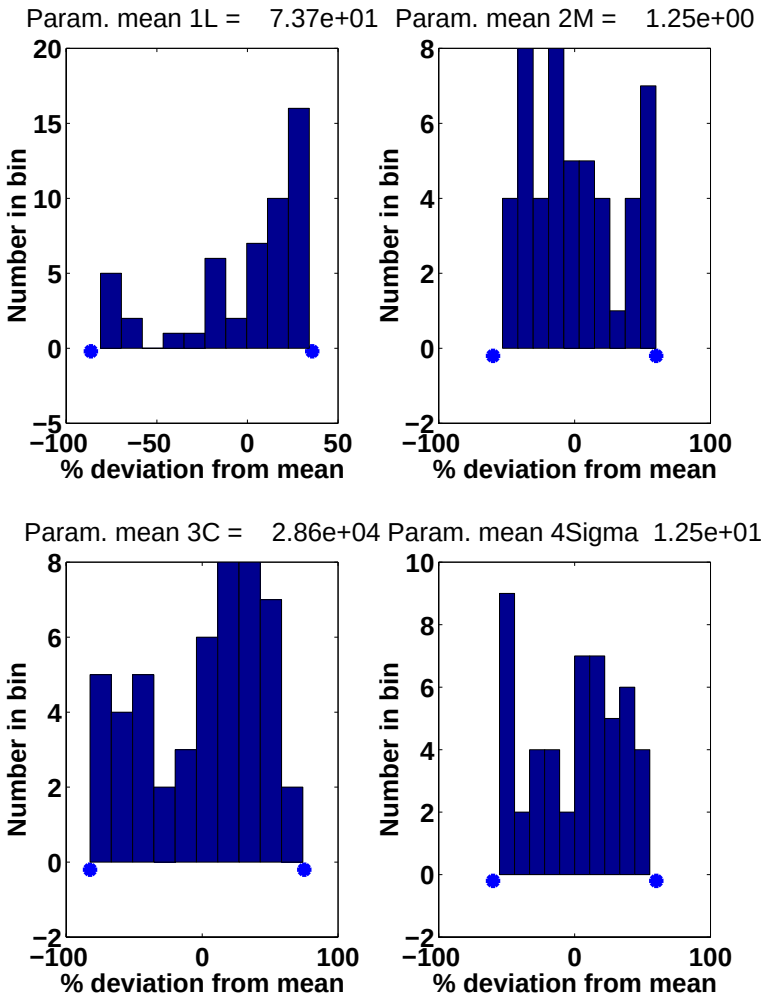

Figure 6: Sample distributions of parameter values for Blanchard–McPherron minimization. The bounds on the distributions correspond to those given in Table 2. The mean values of are listed in Table 3.

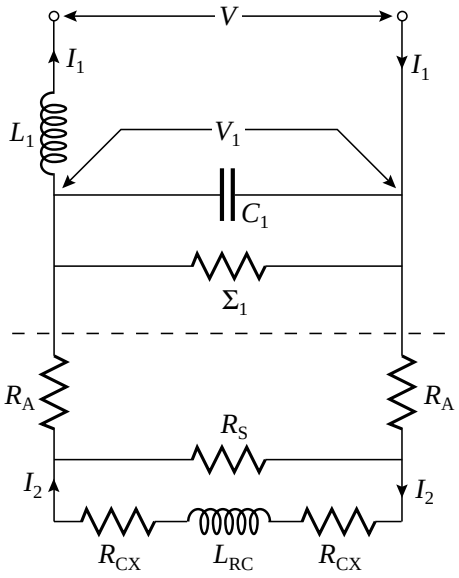

Figure 7: WINDMI coupling to Siscoe circuit. The top part of the circuit (Above dotted line) is the original M-I coupling with the mutual inductance between the ionospheric current loop and lobe loop omitted for clarity. The lower half of the circuit is the coupling to the region 2 loop from Fig. 1 *Siscoe* [1982]

Parameter	Est. Value
L	40.0
M	1.0
C	$1.2 \cdot 10^4$
Σ	40.0
Ω	$1.6 \cdot 10^{24}$
u_o	$6.0 \cdot 10^{-11}$
I_c	$2.2 \cdot 10^7$
α	$1.0 \cdot 10^{12}$
$\tau_{\|}$	$1.0 \cdot 10^3$
τ_E	$1.0 \cdot 10^3$
L_1	12.0
C_1	$1.0 \cdot 10^3$
Σ_I	4.0
β	0.25

Table 1: Estimated values of magnetospheric parameters. All units are MKS.

Parameter	Max. Value	Min. Value
L	100	10
M	2.0	0.5
C	$5.0 \cdot 10^{4}$	$5.0 \cdot 10^{3}$
Σ	20.0	5.0
Ω	$5.0 \cdot 10^{24}$	$5.0 \cdot 10^{23}$
u_o	$5.0 \cdot 10^{-9}$	$5.0 \cdot 10^{-11}$
I_c	$5.0 \cdot 10^{7}$	$5.0 \cdot 10^{6}$
α	$5.0 \cdot 10^{12}$	$5.0 \cdot 10^{11}$
$\tau_{\parallel}$	$1.0 \cdot 10^{3}$	$1.0 \cdot 10^{2}$
τ_E	$5.0 \cdot 10^{3}$	$5.0 \cdot 10^{2}$
L_1	20.0	5.0
C_1	$1.0 \cdot 10^{3}$	$1.0 \cdot 10^{2}$
Σ_I	15.0	5.0
β	0.85	0.10

Table 2: Estimated physical parameter value ranges. The estimates are based on calculations outlined in the text. All units are MKS.

Parameter	Mean Value
L	46.7
M	1.2
C	$2.72 \cdot 10^{4}$
Σ	10.9
Ω	$3.22 \cdot 10^{24}$
u_o	$2.25 \cdot 10^{-9}$
I_c	$3.04 \cdot 10^{7}$
α	$2.06 \cdot 10^{12}$
$\tau_{\parallel}$	523
τ_E	822
L_1	13.6
C_1	525
Σ_1	9.00
β	0.678

Table 3: Mean values of physics parameters (in MKS) determined from the parameter histograms for the Blanchard–McPherron dataset.

Model	$ARV = 1 - PE$	Mean Σ_{Io}	γ_1	γ_2
A	0.93 ± 0.06	9.0		
B	0.71 ± 0.04	9.0	$1.9 \cdot 10^{-10}$	$3.8 \cdot 10^{-8}$

Table 4: Comparison of ionospheric conductivity models found when minimizing over the *Blanchard and McPherron* database. Model B provides improved predictability as seen by the substantial decrease in ARV. The error measure is determined by the standard deviation of the mean ARV over all intervals.

Model	ARV=1–PE	Mean R_A	Mean R_S	Mean R_{cx}	Mean L_{RC}
R2 coupling	0.91 ± 0.06	0.08Ω	11Ω	0.03Ω	$12H$
Reference	0.93 ± 0.06				

Table 5: Summary of results of region 2 coupling model when minimized using the Blanchard and McPherron Dataset. The ARV improvement when a R2 coupling model is included is not statistically significant.The error measure is determined by the standard standard deviation of the mean ARV over all intervals.